



HAL
open science

Filtered Lebedev Quadrature Method for Robust and Efficient Beam Shape Coefficients Estimation in Acoustic Tweezers Calibration

Sarah Vincent, Régis Marchiano, Jean-Louis Thomas

► To cite this version:

Sarah Vincent, Régis Marchiano, Jean-Louis Thomas. Filtered Lebedev Quadrature Method for Robust and Efficient Beam Shape Coefficients Estimation in Acoustic Tweezers Calibration. *Journal of the Acoustical Society of America*, In press, 154 (6), pp.4016-4027. <10.1121/10.0024147>. <hal-04297074>

HAL Id: hal-04297074

<https://hal.science/hal-04297074v1>

Submitted on 21 Nov 2023

HAL is a multi-disciplinary open access archive for the deposit and dissemination of scientific research documents, whether they are published or not. The documents may come from teaching and research institutions in France or abroad, or from public or private research centers.

L'archive ouverte pluridisciplinaire HAL, est destinée au dépôt et à la diffusion de documents scientifiques de niveau recherche, publiés ou non, émanant des établissements d'enseignement et de recherche français ou étrangers, des laboratoires publics ou privés.



HAL Authorization

Filtered Lebedev Quadrature Method for Robust and Efficient Beam Shape Coefficients Estimation in Acoustic Tweezers Calibration

Sarah Vincent,^{1,2} Régis Marchiano,² and Jean-Louis Thomas^{1, a}

¹*Sorbonne Université, CNRS, Institut des Nanosciences de Paris, INSP,
F-75005 Paris, France*

²*Sorbonne Université, CNRS, Institut Jean le Rond d'Alembert, d'Alembert,
F-75005 Paris, France*

(Dated: 21 November 2023)

1 Acoustic tweezers offer a contactless, three-dimensional, and selective approach to
2 trapping objects by harnessing the acoustic radiation force. Precise control of this
3 technique necessitates accurate calibration of the force, which depends on the ob-
4 ject's properties and the spherical harmonics expansion of the incident field through
5 the beam shape coefficients. Previous studies showed that these coefficients can be
6 determined using either the Lebedev quadrature or the angular spectrum methods.
7 However, the former is highly susceptible to noise, while the latter demands extensive
8 implementation time due to the number of required measurement points. A filtered
9 method with reduced number of points is introduced to address these limitations. Ini-
10 tially, we emphasize the implicit filtering in the angular spectrum method, allowing
11 relative noise insensitivity. Subsequently, we present its unfiltered version, enabling
12 force estimation of a standing field. Finally, we develop a filtered method based on
13 the Lebedev quadrature, requiring fewer points and apply it to focused vortex beams.
14 Numerical evaluation of the radiation force demonstrates the method's resilience to
15 noise and a reduced need for points compared to previous method. The filtered
16 Lebedev method paves the way for characterizing high-frequency acoustic tweezers,
17 where measurement constraints necessitate rapid and robust beam shape coefficient
18 estimation techniques.

^aElectronic mail: jean-louis.thomas@sorbonne-universite.fr

19 I. INTRODUCTION

20 Acoustic tweezers recently emerged as a new tool for contactless manipulation of small
21 objects such as cells and molecules. This device is based on radiation force which is the
22 result of the nonlinear interaction of an acoustic field with a solid or fluid obstacle. Many
23 authors^{1,2} have tackled the theoretical expression of this force depending on assumptions,
24 one of them stands out by its generality and few assumptions, which are a linear harmonic
25 propagation and a spherical elastic scatterer³. This theoretical development results in three-
26 dimensional expressions for the radiation force vector which depend on the beam shape
27 coefficients (BSC) of the incident field and on the scattering coefficients of the spherical
28 object. The BSC correspond to the spherical harmonics expansion of the incident acoustic
29 field and the scattering coefficients depend on the object's size and mechanical properties.
30 Theoretical^{3,4} and experimental^{5,6} studies proved that three-dimensional trapping can be
31 achieved by emitting a highly focused vortex beam, giving rise to single beam acoustic
32 tweezers. This kind of field possesses a helical singularity which produces a node pressure
33 on the propagation axis and a strong pressure ring around it.

34 Acoustic tweezers could answer a strong demand in domains such as biophysics as they
35 provide accuracy and accessibility to the sample, compared to standing waves². Many
36 applications can be considered for acoustic tweezers, like the study of biophysical properties
37 of cells and molecules or micro-rheology. For all applications mentioned before, calibration
38 of the radiation force produced by the acoustic tweezers must be conducted. One way of
39 achieving that is to experimentally measure the stiffness of the trap by studying the motions

40 of the trapped object⁷⁻¹², provided that the trapping is easily done. Another indirect way
41 of calibrating the tweezers is to measure its incident field using a calibrated sensor and then
42 use a BSC determination method^{13,14} to finally compute the radiation force for a known
43 scatterer.

44 Two kinds of method have been studied, spatially filtered and unfiltered methods. The first
45 type is based on filtering standing waves, which can be produced by experimental noise in
46 a progressive acoustic beam. This insures that the method is not very sensitive to noise.
47 However, the main existing method, the angular spectrum method^{13,14} (ASM), requires a
48 very high number of measuring points. The second type is not filtering standing waves, like
49 the Lebedev quadrature method¹⁴ which is based on computing the scalar product of the
50 acoustic field with the spherical harmonics on a small optimized set of points. However,
51 this method is very sensitive to noise. The previous studies indicated that the ASM is
52 the most accurate available method, in the presence of noise, to recover the BSC from
53 incident field measurements, but requires a very large number of points. This can be a
54 problem when using an unstable or sensitive measuring sensor, like an interferometer which
55 allows very fine resolution for the measurement of high-frequency focused vortex beams. An
56 optimal method would combine spatial filtering of standing waves and a reduced number of
57 measurement points. Previous works have shown that spherical measurement arrays enable
58 for the accurate reconstruction of noisy acoustic sound fields¹⁵⁻¹⁷ and are thus the geometry
59 studied here. The present work proposes a BSC determination method featuring these two
60 properties. The paper is organized as follows: Section II recalls the developed theory related

61 to acoustic tweezers. Section III highlights the presence of standing wave filtering in the
 62 angular spectrum method. Section IV provides a new optimized filtered method.

63 II. THEORETICAL BACKGROUND

64 A. Radiation force exerted by an arbitrary incident field on an arbitrarily located 65 spherical elastic scatterer

66 Radiation pressure results from the variation of a momentum flux due to the presence
 67 of an obstacle in the propagation path of a sound field. The analytical expressions of the
 68 components of the radiation force exerted on a spherical elastic particle by an arbitrary
 69 sound field are defined in the Cartesian coordinate system (x, y, z) by^{3,13,18}, see also for a
 70 review and for a comparison of the different expressions^{1,19}:

$$F_x = -\frac{\langle V \rangle}{k_0^2} \sum_{n=0}^{\infty} \sum_{m=-n}^n \Im \{ Q_n^{-m} A_n^{m*} A_{n+1}^{m-1} C_n + Q_n^m A_n^m A_{n+1}^{m+1*} C_n^* \}, \quad (1)$$

$$F_y = +\frac{\langle V \rangle}{k_0^2} \sum_{n=0}^{\infty} \sum_{m=-n}^n \Re \{ Q_n^{-m} A_n^{m*} A_{n+1}^{m-1} C_n + Q_n^m A_n^m A_{n+1}^{m+1*} C_n^* \}, \quad (2)$$

$$F_z = -2\frac{\langle V \rangle}{k_0^2} \sum_{n=0}^{\infty} \sum_{m=-n}^n \Im \{ G_n^m A_n^{m*} A_{n+1}^m C_n \}. \quad (3)$$

71 With

$$\begin{aligned}\langle V \rangle &= \frac{p_0^2}{4\rho_0 c_0^2}, \\ C_n &= R_n^* R_{n+1} + 2R_n^* R_{n+1}, \\ Q_n^m &= \sqrt{\frac{(n+m+1)(n+m+2)}{(2n+1)(2n+3)}}, \\ G_n^m &= \sqrt{\frac{(n+m+1)(n-m+1)}{(2n+1)(2n+3)}},\end{aligned}$$

72 where p_0 is the pressure amplitude of the incident field, ρ_0 and c_0 are respectively the density
73 and sound velocity of the surrounding medium, R_n are the scattering coefficients depending
74 only on the sphere radius and its mechanical properties. Finally, A_n^m are the beam shape
75 coefficients (BSC) of the incident field p , corresponding to the amplitude associated to each
76 spherical wave of degree n and order m . These coefficients enable the expansion of the
77 incident field in spherical harmonics such that:

$$p(r, \theta, \varphi) = p_0 \sum_{n=0}^{\infty} \sum_{m=-n}^n A_n^m j_n(k_0 r) Y_n^m(\theta, \varphi), \quad (4)$$

78 with $k_0 = \omega_0/c_0$ the wave number and (r, θ, φ) the spherical coordinates expressed by $x =$
79 $r \sin \theta \cos \varphi$, $y = r \sin \theta \sin \varphi$, $z = r \cos \theta$. The incident field is assumed to be harmonic such
80 that its omitted time dependence is $e^{-i\omega_0 t}$. The spherical harmonics Y_n^m are defined as:

$$Y_n^m(\theta, \varphi) = \sqrt{\frac{2(n+1)(n-m)!}{4\pi(n+m)!}} e^{im\varphi} P_n^m(\cos \theta). \quad (5)$$

81 Computing the radiation force requires knowing the scattering coefficients and the BSC, i.e.
82 knowing the mechanical properties and size of the spherical elastic scatterer, as well as the
83 acoustic incident field.

84 B. Acoustic focused vortex beam for three-dimensional trapping

While the method developed here for the BSC reconstruction from measurements is general, it will be illustrated in the context of single beam acoustic tweezers. The main advantages of this type of field for contactless acoustic manipulation are the three-dimensionality, selectivity and accuracy of the trap. Depending on the contrast factor between the object and the medium the trap may require a minimum or a maximum of intensity at the focus. For instance, stiffer and heavier particles are attracted to areas of negative gradient, i.e. to the pressure nodes. Three dimensional trapping has been demonstrated numerically^{3,4} and experimentally^{5,20} using focused acoustical vortices. The axial force generated by acoustical vortices of order 0²¹, 1²² and higher²³ has been studied previously, see also²⁴. The focused acoustic vortex beam can be expanded in spherical harmonics by Eq (4), with⁴:

$$\begin{aligned}
 A_n^{m,th} &= \delta_{m,m'} 4\pi (k_0 r_0)^2 N_n^{m'} h_n^{(1)}(k_0 r_0) \\
 &\times \int_{\pi-\alpha_0}^{\pi} P_n^{m'}(\cos \theta') \sin \theta' d\theta', \\
 \delta_{m,m'} &= \begin{cases} 1 & \text{if } m = m' \\ 0 & \text{if } m \neq m', \end{cases}
 \end{aligned} \tag{6}$$

the BSC of the incident focused vortex field propagating along the z direction. These coefficients are non-zero only for the order $m = m'$. In this study $m' = 1$, although higher topological charges also allow contactless manipulation^{3,6,25}. The parameters r_0 and α_0 are respectively the focusing distance and the aperture angle.

The BSC of the focused vortex, computed for a 50 MHz frequency in water ($c_0 = 1497$ m/s and $\rho_0 = 997$ kg/m³), a topological charge $m' = 1$, $r_0 = 3$ mm and $\alpha_0 = 50^\circ$, are shown

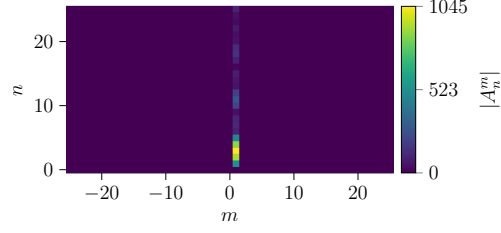
100 Fig. 1 (A). The associated pressure field is rendered Fig. 1 (B). Finally, the cylindrical com-
 101 ponents of the radiation force exerted on a spherical silica bead (of density $\rho_p = 2200 \text{ kg/m}^3$,
 102 longitudinal velocity $c_L = 5800 \text{ m/s}$ and transverse velocity $c_T = 3500 \text{ m/s}$) of radius 0.2λ ,
 103 with $\lambda = c_0/f_0$ the acoustic wavelength, about $30 \mu\text{m}$, are plotted Fig. 1 (C). The lateral
 104 forces, F_ρ and F_φ cancel at the origin. The radial force exhibits a negative part away from
 105 the centre, tending to attract the bead towards it. The azimuthal force tends to rotate the
 106 bead when moved away from the centre. The axial force acts as a restoring force as the parts
 107 on either side of the centre are directed towards it, thus establishing a three-dimensional
 108 equilibrium position allowing selectivity.

110 C. Beam shape coefficients (BSC) determination

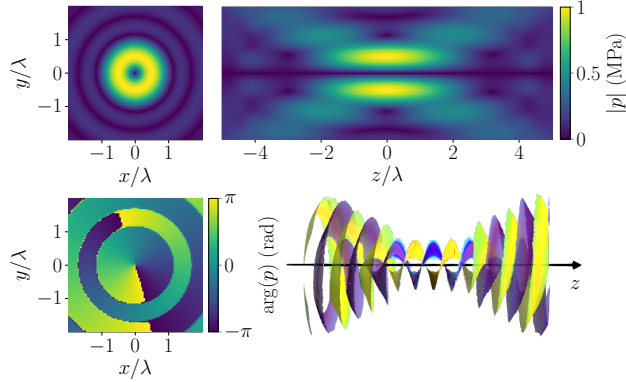
111 The scattering coefficients C_n in Eqs. (1)-(3) can be computed analytically from the
 112 values of the mechanical properties and size of the spherical elastic scatterer³. The task is
 113 then reduced to the computation of the BSC of the incident field. Several methods have
 114 been explored^{13,14} and fall into two main categories: unfiltered methods and spatially filtered
 115 methods.

116 1. *Unfiltered method: Lebedev quadrature*

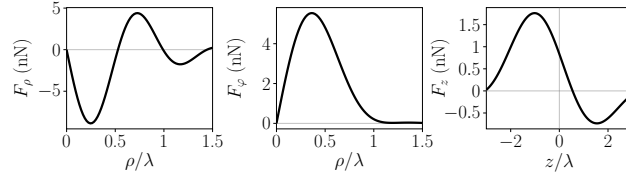
Using the orthogonality property of the spherical harmonics, the beam shape coefficients
 117 can be expressed from the incident pressure field:



(A) Modulus of the beam shape coefficients.



(B) Modulus (top) and phase (bottom) of the pressure field.



(C) Cylindrical components of the radiation force.

FIG. 1. (Color online) Highly focused acoustic vortex beam propagating along z at a 50 MHz frequency in water. (A) Beam shape coefficients of the focused vortex of topological charge $m' = 1$, focusing distance $r_0 = 3$ mm and aperture angle $\alpha_0 = 50^\circ$. (B) Modulus (top) and phase (bottom) of the pressure field in the transverse (left) and axial (right) planes. The maximum pressure amplitude is set to 1 MPa. (C) Radiation force exerted on a $7 \mu\text{m}$ radius silica bead. The lateral components F_ρ and F_φ are computed for $z = 0$ and the axial component F_z for $\rho = 0$ in the cylindrical coordinate system.

118

$$\begin{aligned}
A_n^m &= \frac{1}{p_0 j_n(k_0 r)} \langle p, Y_n^m \rangle, \\
&= \frac{1}{p_0 j_n(k_0 r_S)} \int_{\theta=0}^{\pi} \int_{\varphi=0}^{2\pi} p(r_S, \theta_S, \varphi_S) \\
&\quad \times Y_n^{m*}(\theta_S, \varphi_S) \sin \theta_S \, d\theta_S \, d\varphi_S,
\end{aligned} \tag{7}$$

119 with $p(r_S, \theta_S, \varphi_S)$ the incident pressure field measured on a sphere of radius r_S .

120 A way to approximate the surface integral on the sphere is to use the Lebedev quadrature²⁶.

121 To compute the force, series are truncated at order $N = 25$. To be consistent, the number

122 of points used in the Lebedev quadrature has to be 975²⁷. However, this method is very

123 sensitive to noise. As the scalar product is a linear operation, the complete result is the

124 sum of the scalar product with the theoretical field and the scalar product with the noise.

125 Thus, the method has an error proportional to $1/j_n(k_0 r_S)$, which can be very high for some

126 integrating sphere radii r_S . Indeed, the noise is strongly amplified when j_n approaches 0

127 for some r_S . In particular for $j_0(kr_s) = \sin(kr_s)/(kr_s)$ when $r_S/\lambda = l/2$, with $l \in \mathbb{N}^+$. The

128 estimation of the force with this method can therefore work if the radius of the integrating

129 sphere is well chosen, for example $r_S = 5.6\lambda$ ¹⁴. On the other hand, if the radius corresponds

130 to the cancellation of j_n , e.g. for $r_S = 7\lambda$, then the error explodes for each component of

131 the force.

132 In the case of such problematic sphere radii, it is possible to reduce the error by cancelling

133 the A_0^0 term of the BSC. Then the error remains relatively small and the estimated force

134 approaches its theoretical value. However it has been shown¹⁴ that the axial component

135 shows oscillations. These oscillations have a period close to half a wavelength suggesting the

136 presence of standing waves, presumably produced by the addition of random noise to the

137 acoustic field. Moreover it is known that standing waves tend to produce stronger radiation
 138 forces than progressive waves²⁸. Thus filtering of the standing waves, in the case of the
 139 progressive field, is optimal for the estimation of the radiation force from the determination
 140 of the BSC¹⁴.

141 **2. Filtered method: Angular spectrum method (ASM)**

142 A filtered method for the determination of the BSC, applied to a progressive beam,
 143 consists in spatially filtering the standing waves components resulting from the presence of
 144 noise. The angular spectrum method^{13,14} (ASM), based on the plane wave expansion of the
 145 incident field and on the Fourier transform, implements an implicit filtering of the standing
 146 waves, which will be demonstrated in section III. First a reminder of the ASM¹³ is given.
 147 If the acoustic field is known in a transverse plane, arbitrarily chosen in $z = 0$, and is an
 148 integrable function then the two-dimensional spectrum or angular spectrum is:

$$S_0(k_x, k_y) = \iint_{-\infty}^{\infty} p(x, y, z = 0) e^{-i(k_x x + k_y y)} dx dy. \quad (8)$$

149 Then the pressure field at any position z is defined by:

$$p(x, y, z) = \frac{1}{(2\pi)^2} \iint_{k_x^2 + k_y^2 \leq k_0^2} S_0(k_x, k_y) e^{ik_z z} e^{i(k_x x + k_y y)} dk_x dk_y, \quad (9)$$

150 where $k_z = \sqrt{k_0^2 - k_x^2 - k_y^2}$. The integral limit stems from the dispersion relation and results
 151 in the filtering of evanescent waves. Then, from the plane wave expansion of the integrand
 152 $e^{i\vec{k}\cdot\vec{r}}$ in spherical coordinates:

$$e^{i\vec{k}\cdot\vec{r}} = 4\pi \sum_{n=0}^{\infty} \sum_{m=-n}^n i^n j_n(k_0 r) Y_n^m(\theta, \varphi) Y_n^{m*}(\theta_k, \varphi_k), \quad (10)$$

153 where $\theta_k = \arccos(k_z/k_0)$ and $\varphi_k = \arctan(k_y/k_x)$ and its injection in Eq. (9), the BSC are
 154 identified using Eq. (4):

$$A_n^m = \frac{i^n}{\pi} \iint_{k_x^2 + k_y^2 \leq k^2} S_0(k_x, k_y) Y_n^{m*}(\theta_k, \varphi_k) dk_x dk_y. \quad (11)$$

155 Note that the pressure amplitude coefficient p_0 is now included in the BSC. This method
 156 requires knowledge of the sound field on a sufficiently large and fine mesh, otherwise inte-
 157 gration errors may occur. In the case of an adequate mesh, the reconstructed BSC are in
 158 good agreement with the theoretical ones for $m = m'$ the topological charge of the vortex,
 159 but noisy elsewhere. The reconstructed force does not exhibit oscillations, unlike the first
 160 unfiltered method¹⁴.

161 III. IMPLICIT FILTERING IN THE ASM

162 We propose to demonstrate that the ASM¹³, recalled in section II C 2, is implicitly using
 163 a spatial filtering of the standing waves. Then, an unfiltered ASM will be developed.

164 A. Application to a standing wavefield

165 The ASM is applied to a standing field, defined by the following BSC:

$$A_n^{m,stat} = \frac{1}{2} \left[A_n^{m,th} + (A_n^{m,th} e^{i\pi})^* \right], \quad (12)$$

166 where $A_n^{m,th}$ are the theoretical BSC defined by Eq. (6) for the progressive focused vortex,
 167 and $A_n^{m,th*}$ their conjugates. Once again, note that the theoretical BSC are including the
 168 pressure amplitude coefficients p_0 , therefore their amplitude is different from the ones shown

169 Fig. 1 (A). The resulting maximal amplitude of the progressive pressure field is 1 MPa, as
 170 well as for the standing pressure field, due to the 1/2 coefficient in Eq. (12).

171 The BSC $A_n^{m,stat}$ associated with the standing field are shown Fig. 2 (A). The main effect of
 172 standing waves features appears along the $m = m' = 1$ axis where the $A_n^{m'}$ are discontinuous
 173 compared to the progressive version (cf. Fig 1 (A)). This can be explained by Eq. (4) and the
 174 following parity property of the associated Legendre polynomials involved in the spherical
 175 harmonics, Eq. (5):

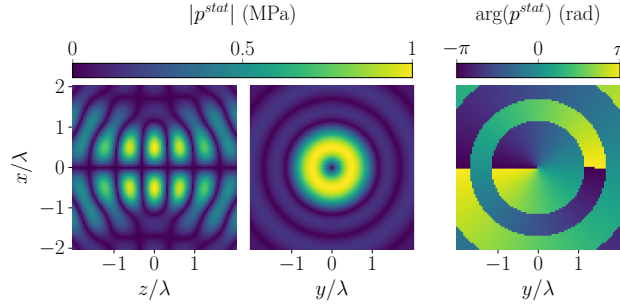
$$P_n^m(-x) = (-1)^{n+m} P_n^m(x) \quad (13)$$

176 where $x = \cos \theta$, and the angle $\pi - \theta$ corresponds to the direction opposite to that of the
 177 progressive field. One coefficient out of every two will therefore cancel and the other will
 178 be added, hence the 1/2 factor in Eq. (12). The resulting pressure field, Fig. 2 (B), does
 179 show standing waves features along the propagation axis z .

180 In order to demonstrate the implicit filtering of standing waves components, the angular
 182 spectrum recalled section II C 2 defined by Eq. (11) is applied to the "standing focused vor-
 183 tex", i.e the superposition of two counterpropagating focused vortex, described previously.
 184 To do so, the theoretical BSC, Eq. (12), are used to compute the pressure field from Eq. (4)
 185 onto a plane at $z = 0$ of dimensions $6\lambda \times 6\lambda$ and 3721 points, corresponding to a spatial
 186 sampling of $\lambda/10$. As seen Fig. 2 (B), the resulting maximum pressure amplitude P_{max} of
 187 the field is 1 MPa around the focus. To match real experimental conditions, random noise is
 188 then added to the pressure field and its maximum amplitude is 5% of P_{max} . Finally, Eq. (11)
 189 is employed to estimate the BSC, which are plotted Fig. 3. It appears that the ASM does
 190 not render the standing wavefield. The obtained BSC are closer to the progressive version



(A) Modulus of the BSC.



(B) Modulus (left) and phase (right) of the pressure field.

FIG. 2. (Color online) Theoretical BSC and pressure field of the standing focused vortex beam defined by Eq. (12). The pressure field is plotted in the propagation plane (Oxz) and in the transverse plane (Oxy) as well.

192 of the field (cf. Fig. 1 (A)) indicating an implicit filtering of the standing waves.

193 B. Unfiltered ASM

194 The implicit filtering of standing waves can be removed from the previous ASM. The
 195 starting point is the three-dimensional Fourier transform of the harmonic acoustic field:

$$\text{TF}_{3\text{D}}[p(\vec{r})] = P(\vec{k}) = \int_{\vec{r} \in \mathbb{R}^3} p(\vec{r}) e^{-i\vec{k} \cdot \vec{r}} d^3\vec{r}, \quad (14)$$

196 where $\vec{r} = x\vec{e}_x + y\vec{e}_y + z\vec{e}_z$ is the spatial coordinates vector, and $\vec{k} = k_x\vec{e}_x + k_y\vec{e}_y + k_z\vec{e}_z$

197 the wave vector. The field being solution of the Helmholtz equation, the dispersion relation

198 $k_x^2 + k_y^2 + k_z^2 = k_0^2$, with $k_0 = \omega_0/c_0$, imposes

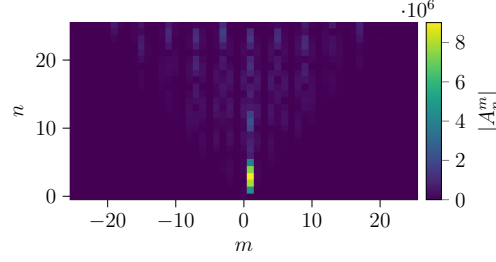


FIG. 3. (Color online) Modulus of the BSC of the standing focused vortex field (cf. Fig 2 (A)) estimated using the filtered ASM, Eq. (11), on the plane located in $z = 0$ of dimensions $6\lambda \times 6\lambda$ sampled in 3721 points.

$$k_z = \pm \sqrt{k_0^2 - k_x^2 - k_y^2} = \pm q. \quad (15)$$

199 Then, Eq. (14) becomes:

$$\text{TF}_{3\text{D}} [p(\vec{r})] = P(\vec{k}) [\delta(k_z - q) + \delta(k_z + q)]. \quad (16)$$

200 The sound field is simply the inverse Fourier transform of P such that:

$$p(\vec{r}) = \frac{1}{(2\pi)^3} \int_{\vec{k} \in \mathbb{R}^3} P(\vec{k}) e^{i\vec{k} \cdot \vec{r}} d^3\vec{k}. \quad (17)$$

Using the plane wave expansion Eq. (10) and applying the dispersion relation (cf. Eq. (15)),

201 Eq. (17) becomes:

$$\begin{aligned} p(\vec{r}) &= \sum_{n=0}^{\infty} \frac{i^n}{2\pi^2} j_n(k_0 r) \sum_{m=-n}^n Y_n^m(\vec{r}) \\ &\times \iint_{k_x^2 + k_y^2 \leq k_0^2} [P(k_x, k_y, q) Y_n^{m*}(k_x, k_y, q) \\ &+ P(k_x, k_y, -q) Y_n^{m*}(k_x, k_y, -q)] dk_x dk_y, \end{aligned}$$

The spherical harmonics can be written as $Y_n^{m*}(\theta_k, \varphi_k)$ with $\cos \theta_k = k_z/k_0$ and $\tan \varphi_k =$

202 k_y/k_x . The associated Legendre polynomials parity Eq. (13) with $x = \cos \theta_k = k_z/k_0 =$
 203 $\pm q/k_0$ yields:

$$p(\vec{r}) = \sum_{n=0}^{\infty} \frac{i^n}{2\pi^2} j_n(k_0 r) \sum_{m=-n}^n Y_n^m(\vec{r})$$

$$\times \iint_{k_x^2 + k_y^2 \leq k_0^2} [P^+ + (-1)^{n+m} P^-] Y_n^{m*}(k_x, k_y, q) dk_x dk_y,$$

204 where $P^+ = P(k_x, k_y, q)$ corresponds to the progressive part of the field and $P^- =$
 205 $P(k_x, k_y, -q)$ to its regressive part. The BSC are identified using the spherical harmon-
 206 ics expansion of the field (cf. Eq. (4)):

$$A_n^m = \frac{i^n}{2\pi^2} \iint_{k_x^2 + k_y^2 \leq k_0^2} [P^+ + (-1)^{n+m} P^-]$$

$$\times Y_n^{m*}(k_x, k_y, q) dk_x dk_y. \quad (18)$$

Comparing Eq. (8) with Eqs. (14), (15) and (16), the angular spectrum is defined as the
 207 inverse Fourier transform of $P(k_x, k_y, k_z)$ with respect to k_z :

$$S_z(k_x, k_y) = \frac{1}{2\pi} \int_{-\infty}^{+\infty} P(k_x, k_y, k_z) e^{ik_z z} dk_z,$$

$$= \frac{1}{2\pi} [P^+ e^{iqz} + P^- e^{-iqz}].$$

208 For a progressive wave along the +z-direction, $S_{z=0}(k_x, k_y) = P^+/(2\pi)$, with $S_{z=0}$ the angular
 209 spectrum of the acoustic field at plane $z = 0$. From Eq. (18), one thus finds the expression
 210 of the BSC given by the filtered ASM¹³ (cf. Eq. (11)):

$$A_n^m = \frac{i^n}{\pi} \iint_{k_x^2 + k_y^2 \leq k_0^2} S_{z=0}(k_x, k_y) Y_n^{m*}(\theta_k, \varphi_k) dk_x dk_y, \quad (19)$$

For an arbitrary wave, P^+ and P^- must be accounted for, it is then necessary to know

211 the angular spectrum on two different planes $z = z_1$ and $z = z_2$:

$$\begin{cases} S_{z_1}(k_x, k_y) = \frac{1}{2\pi} [P^+ e^{iqz_1} + P^- e^{-iqz_1}], \\ S_{z_2}(k_x, k_y) = \frac{1}{2\pi} [P^+ e^{iqz_2} + P^- e^{-iqz_2}]. \end{cases}$$

212 Leading to:

$$\begin{cases} (e^{2iqz_1} - e^{2iqz_2}) P^+ = 2\pi (S_{z_1} e^{iqz_1} - S_{z_2} e^{iqz_2}), \\ (e^{-2iqz_1} - e^{-2iqz_2}) P^- = 2\pi (S_{z_1} e^{-iqz_1} - S_{z_2} e^{-iqz_2}). \end{cases} \quad (20)$$

213 Replacing the pair (P^+, P^-) by (S_{z_1}, S_{z_2}) requires avoiding cases where either $(e^{2iqz_1} - e^{2iqz_2})$

214 or $(e^{-2iqz_1} - e^{-2iqz_2})$ cancels, see discussion below. By injecting these expressions in Eq. (18):

$$\begin{aligned} A_n^m = \frac{i^n}{\pi} \iint_{k_x^2 + k_y^2 \leq k_0^2} & \left[\frac{S_{z_1} e^{iqz_1} - S_{z_2} e^{iqz_2}}{e^{2iqz_1} - e^{2iqz_2}} \right. \\ & \left. + (-1)^{n+m} \frac{S_{z_1} e^{-iqz_1} - S_{z_2} e^{-iqz_2}}{e^{-2iqz_1} - e^{-2iqz_2}} \right] Y_n^{m*} dk_x dk_y. \end{aligned} \quad (21)$$

215 *A priori*, the choice of planes z_1 and z_2 is arbitrary, here they are chosen symmetrically

216 around the origin, such that $z_1 = -z$ and $z_2 = z$, with $z > 0$, so:

$$\begin{aligned} A_n^m = \frac{i^n}{\pi} \iint_{k_x^2 + k_y^2 \leq k_0^2} & \frac{1}{2i \sin(2qz)} \\ & \times [S_{z^+} (e^{iqz} - (-1)^{n+m} e^{-iqz}) \\ & - S_{z^-} (e^{-iqz} - (-1)^{n+m} e^{iqz})] Y_n^{m*} dk_x dk_y. \end{aligned} \quad (22)$$

217 When $(-1)^{n+m} = 1$:

$$A_n^m = \frac{i^n}{\pi} \iint_{k_x^2 + k_y^2 \leq k_0^2} \left[\frac{S_{z^+} + S_{z^-}}{2 \cos(qz)} \right] Y_n^{m*} dk_x dk_y, \quad (23)$$

218 and when $(-1)^{n+m} = -1$:

$$A_n^m = \frac{i^n}{\pi} \iint_{k_x^2 + k_y^2 \leq k_0^2} \left[\frac{S_{z^+} - S_{z^-}}{2i \sin(qz)} \right] Y_n^{m*} dk_x dk_y. \quad (24)$$

219 As noted above, either $\cos(qz) = 0$ or $\sin(qz) = 0$ may occur. We recognize here special
 220 cases like symmetrical and antisymmetrical standing waves with nodes on the chosen planes.
 221 To avoid such possibility, a simple solution is to select $0 < qz < \pi/2$, so $0 < z < \lambda/4$ since
 222 $q < 2\pi/\lambda$. In the limiting case where z tends toward 0, we recover the case of one single
 223 plane at $z = 0$. In this case, Eq. (23) becomes the one obtained in Ref.¹³ (see Eq. (11)).
 224 While Eq. (24) is new and similar, but S_z is replaced by $(1/iq) dS_z/dz$. Thus the field can
 225 be computed everywhere if it is known, as well as its normal derivative, on a plane.

226 Unlike the filtered method, this complete ASM should be able to estimate the BSC of
 227 a standing wavefield like the one defined by Eq. (12). To do so, the theoretical field is
 228 computed on two planes taken in $z = -0.1\lambda$ and $z = 0.1\lambda$, their dimensions are $6\lambda \times 6\lambda$ and
 229 the number of points is 3721. As before, random noise is numerically added to the pressure
 230 field at 5% of its maximum amplitude. The BSC are then estimated using Eq. (22). The
 231 reconstructed radiation force is plotted Fig. 4 and compared to the theoretical one and the
 232 one obtained from the filtered ASM.

233 The errors made by each method on the force estimation are defined as:

$$\epsilon(F_\gamma, x) = \frac{100}{N_x} \sum_{j=0}^{N_x-1} \frac{|F_\gamma(x_j) - F_\gamma^{th}(x_j)|}{\max|F_\gamma^{th}|} \quad (\%), \quad (25)$$

234 with $\{F_\gamma, x\} = \{F_\rho, \rho\}, \{F_\varphi, \rho\}, \{F_z, z\}$. As planned, only the unfiltered method recovers
 235 the proper force. Furthermore, at equivalent pressure amplitude between the standing and
 236 progressive fields, the axial force of the standing wave is twice as large, with respect to the
 237 positive peak, and six times larger, with regard to the negative peak. The standing waves
 238 therefore have a substantial contribution to the radiation force²⁸. The amplitude distribution
 239 between the positive and negative peaks of the axial force is balanced. Although slightly

240 overestimated by the filtered methods, the radial force is hardly modified compared to the
 241 progressive vortex (cf. Fig 1 (C)). Indeed, the latter already has a standing wave behavior
 242 due to the focusing of the field. This amplitude ratio will also depends on the focusing
 243 sharpness or aperture angle α_0 . The azimuthal component, on the other hand, maintains a
 244 progressive behavior.

245

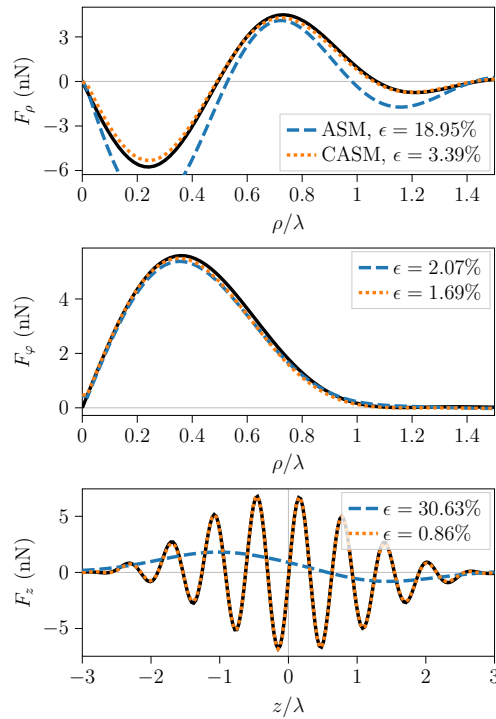


FIG. 4. (Color online) Estimation of the cylindrical components of the radiation force exerted on a $7 \mu\text{m}$ silica bead by a standing focused vortex beam (defined by Eq. (12)) using the filtered ASM (Eq (11)) and the unfiltered complete ASM (noted CASM) (Eq.(22)) on a plane located in $z = 0$ for the ASM, and on 2 planes located in $z = \pm 0.1\lambda$ for the CASM. Each plane has dimensions $6\lambda \times 6\lambda$ and is sampled in 3721 points. The theoretical force is plotted in black. The errors ϵ made by each method on the force are given by Eq. (25).

246

247 **IV. NEW BSC DETERMINATION METHOD : FILTERED LEBEDEV METHOD**

248 The existing methods described in section II C are either very sensitive to noise, or very
 249 costly in terms of measurement duration, due to the large number of points required to
 250 compute the BSC. These two aspects can be particularly problematic when the measurement
 251 is noisy or subject to deterioration over the duration of the measurement.

252 The Lebedev method described in section II C 1 seemed promising given the reduced number
 253 of measurement points and their distance from the focal spot, where the dynamics of the
 254 measured signals are important. However, it is too sensitive to noise. An improvement of
 255 this method would be to add filtering. Indeed, the presence of noise in the acoustic field
 256 acts like the presence of a standing wave and filtering this standing wave would reduce the
 257 impact of noise on a progressive field. The ASM, which already uses this type of filtering
 258 (cf. section III A), is much more robust to noise than the unfiltered Lebedev method. The
 259 theoretical development for applying standing wave filtering is described below.

260 **A. Theoretical development**

261 The starting point of this filtered Lebedev method is to consider a harmonic acoustic field
 262 propagating linearly in a homogeneous perfect fluid without any source. Thus, the acoustic
 263 field $\Psi(\vec{r})$ verifies the homogeneous Helmholtz equation:

$$(\Delta + k^2)\Psi(\vec{r}) = 0, \quad (26)$$

264 where $\Psi(\vec{r})$ is the spatial dependence of the field and $e^{-i\omega_0 t}$ its implicit time dependence.

265 This equation can be solved using the Green function $G(\vec{r}|\vec{r}_S) = G$, solution of:

$$(\Delta + k^2)G = -\delta(\vec{r} - \vec{r}_S). \quad (27)$$

266 The acoustic field is then written²⁹:

$$\Psi(\vec{r}) = \iint_S [G\nabla\Psi(\vec{r}_S) \cdot \vec{n} - \Psi(\vec{r}_S)\nabla G \cdot \vec{n}] dS. \quad (28)$$

267 It is determined in the volume contained by S , an arbitrary closed surface with outward

268 unit normal \vec{n} . In order to have a unique solution, a boundary conditions on S is required,

269 for instance Dirichlet, Ψ is fixed on S or Neumann conditions where $\nabla\Psi \cdot \vec{n}$ is given instead.

270 The homogeneous version of this condition should be used to determine the Green function,

271 G . In Kirchhoff approach both Ψ and $\nabla\Psi \cdot \vec{n}$ are fixed on S and the Green function is the

272 Green function of free space, G_0 Eq. (29).

$$G = G_0 = \frac{e^{ik_0 R}}{4\pi R}, \text{ where } R = |\vec{r} - \vec{r}_S|. \quad (29)$$

273 In the following, to simplify the presentation, the closed surface S is chosen as a fictitious

274 spherical surface of radius r_S . Thus $\nabla(\cdot) \cdot \vec{n} = \partial(\cdot)/\partial r$. The spherical harmonics expansion

275 of the free space Green function G_0 , for $r_S > r$ is given by³⁰:

$$G_0 = ik_0 \sum_{n,m} j_n(k_0 r) h_n^{(1)}(k_0 r_S) Y_n^{m*}(\theta_S, \varphi_S) Y_n^m(\theta, \varphi), \quad (30)$$

276 where $(r_S, \theta_S, \varphi_S)$ are the spherical coordinates describing S and $\sum_{n,m} = \sum_{n=0}^{\infty} \sum_{m=-n}^n$.

277 Thus,

$$\begin{aligned} \left. \frac{\partial G_0}{\partial r'} \right|_{r'=r_S} &= ik_0 \sum_{n,m} j_n(k_0 r) \left. \frac{\partial h_n^{(1)}(k_0 r')}{\partial r'} \right|_{r'=r_S} \\ &\times Y_n^{m*}(\theta_S, \varphi_S) Y_n^m(\theta, \varphi). \end{aligned} \quad (31)$$

278 Injecting these last equations in Eq. (28), it becomes:

$$\begin{aligned} \Psi(r, \theta, \varphi) = & -ik_0 \sum_{n,m} j_n(k_0 r) Y_n^m(\theta, \varphi) \\ & \times \int_0^{2\pi} \int_0^\pi \left[\Psi_S \frac{\partial h_n^{(1)}}{\partial r'} \Big|_{r'=r_S} - h_n^{(1)}(k_0 r_S) \frac{\partial \Psi}{\partial r'} \Big|_{r'=r_S} \right] \\ & \times Y_n^{m*}(\theta_S, \varphi_S) r_S^2 d\Omega, \end{aligned} \quad (32)$$

279 where $\Psi_S = \Psi(r_S, \theta_S, \varphi_S)$ and $d\Omega = \sin \theta_S d\theta_S d\varphi_S$. Comparing with Eq. (4) to the difference
280 that the amplitude coefficient ψ_0 (or p_0 in pressure) is included in the BSC yields :

$$A_n^m = -ik_0 r_S^2 \left\langle \Psi \frac{\partial h_n^{(1)}}{\partial r'} \Big|_{r'=r_S} - h_n^{(1)} \frac{\partial \Psi}{\partial r'} \Big|_{r'=r_S}, Y_n^m \right\rangle. \quad (33)$$

281 To facilitate the comparison, we use the notation $\langle \cdot, \cdot \rangle$ of Eq. (7) in place of the integral. We
282 can check its consistency using the expansion of $\Psi(\vec{r})$ in spherical harmonics with another
283 set of BSC:

$$\Psi(r, \theta, \varphi) = \sum_{n,m} B_n^m j_n(k_0 r) Y_n^m(\theta, \varphi), \quad (34)$$

284 From this expansion, the field on the surface S and its derivative are obtained and injected
285 in Eq. (33). Permuting series and integrals signs and using the orthogonality of the Y_n^m ,
286 yields:

$$A_n^m = -ix^2 B_n^m \left[j_n(x) \frac{dh_n^{(1)}(x)}{dx} - \frac{dj_n(x)}{dx} h_n^{(1)}(x) \right] \quad (35)$$

287 where $x = k_0 r_S$. Using the definition $h_n^{(1)}(x) = j_n(x) + iy_n(x)$, the bracket of Eq. (35) can
288 be rewritten as $i [j_n(x)y_n'(x) - j_n'(x)y_n(x)]$ where prime stands for derivative. We recognize
289 a Wronskian whose value is $(1/x^2)^{31}$ (Chap. 10, Eq. (10.1.6)). We can then confirm the
290 consistency of Eq. (35) since we obtain, as expected from the uniqueness of the solution:
291 $A_n^m = B_n^m$. Note that we chose to replace $h_n^{(1)}(x)$ and its derivative in the bracket. Another

292 equivalent choice is to replace j_n and its derivative using $2j_n(x) = h_n^{(1)}(x) + h_n^{(2)}(x)$. In this
 293 last case the bracket becomes $(1/2) [h_n^{(2)}(x)h_n'^{(1)}(x) - h_n'^{(2)}(x)h_n^{(1)}(x)]$. This shows that even
 294 if Ψ , as written in Eq. (34), involves j_n and hence the sum of the two Hankel functions, only
 295 the incoming part, $h_n^{(2)}$, makes a contribution to the value of the A_n^m while the other part
 296 involving $h_n^{(1)}$ cancels out.

297 Eq. (33) requires the knowledge of both the field and its radial derivative on a closed
 298 surface. First, this is not always possible to measure the field and its derivative. Second,
 299 assigning a value to both is unnecessary since they are related, see for a review³². For single-
 300 beam acoustic tweezers the field is progressive and hence enters the surface on the upstream
 301 side and leaves on the downstream side, as shown in Fig. 5. For a surface sufficiently far

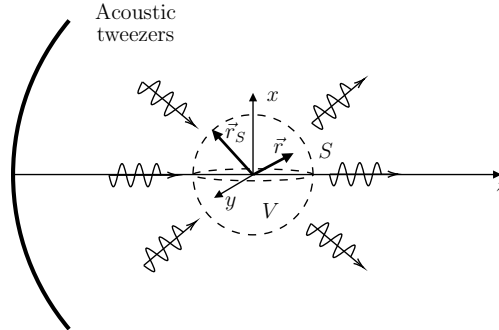


FIG. 5. Configuration of the filtered Lebedev method: if the field is progressive, it is entering the volume where $\theta \in [\pi/2, \pi]$ and outgoing when $\theta \in [0, \pi/2]$, where $\theta = \arccos(r/z)$.

302

303

304 from the area of interest, $k_0 r_S \gg 1$, these boundary conditions are enforced by Sommer-
 305 feld radiation conditions³³. With the convention chosen here $\exp(-i\omega t)$, if $\theta_S \in [0, \frac{\pi}{2}]$, i.e

306 downstream:

$$\left. \frac{\partial \Psi_S}{\partial r'} \right|_{r'=r_S} \approx \left(+ik_0 - \frac{1}{r_S} \right) \Psi_S \quad (36)$$

307 while for upstream, $\theta_S \in [\frac{\pi}{2}, \pi]$

$$\frac{\partial \Psi_S}{\partial r'} \Big|_{r'=r_S} \approx (-ik_0 - \frac{1}{r_S}) \Psi_S \quad (37)$$

This last condition, Eq. (36) for outgoing wave, is satisfied by $h_n^{(1)}$ on the whole surface,
 308 with $h_n^{(1)}(x) \approx i^{-n-1} \exp(ix)/x^{31}$. This approximation holds for $k_0 r_S \geq 2N$, especially for
 309 the phase of the Hankel functions. Corollary, $h_n^{(2)}$ satisfy Eq. (37) for incoming wave. Using
 310 these boundary conditions, Eqs. (36),(37) for the field Ψ and the derivative of the Hankel
 311 function, Eq. (33) can be rewritten:

$$\begin{aligned} A_n^m = & -ik_0 r_S^2 \int_0^{2\pi} \left\{ \int_{\frac{\pi}{2}}^{\pi} \left[(ik_0 - \frac{1}{r_S}) h_n^{(1)}(k_0 r_S) \Psi_S \right. \right. \\ & \left. \left. - h_n^{(1)}(k_0 r_S) (-ik_0 - \frac{1}{r_S}) \Psi_S \right] Y_n^{m*}(\theta_S, \varphi_S) d\Omega \right. \\ & \left. + \int_0^{\frac{\pi}{2}} \left[(ik_0 - \frac{1}{r_S}) h_n^{(1)}(k_0 r_S) \Psi_S \right. \right. \\ & \left. \left. - h_n^{(1)}(k_0 r_S) (ik_0 - \frac{1}{r_S}) \Psi_S \right] Y_n^{m*}(\theta_S, \varphi_S) d\Omega \right\}, \end{aligned}$$

312 In the second integral, the sum of the two terms cancels out so that finally:

$$A_n^m = 2k_0^2 r_S^2 h_n^{(1)}(k_0 r_S) \int_0^{2\pi} \int_{\frac{\pi}{2}}^{\pi} \Psi_S Y_n^{m*}(\theta_S, \varphi_S) d\Omega \quad (38)$$

313 Eq. (38) requires knowing the field on half the surface, the upstream side. This last feature
 314 comes from the noted fact that only the $h_n^{(2)}$ part of j_n contributes to Eq. (35), combined
 315 with the boundary conditions Eqs. (36),(37), imposing an incoming field on a single side.
 316 Thus by enforcing these conditions, even if the measured field is noisy, the noise can only
 317 add random fluctuations on the upstream side. Without the incoming contribution from the

318 downstream side, the noise standing wave content is filtered out.

319 It is advantageous compared to the ASM because it uses the optimized set of points on
 320 the sphere, given by the Lebedev quadrature, and it is sufficient to measure the acoustic field
 321 on the fictitious half-sphere between $\theta_S = \pi/2$ and $\theta_S = \pi$, which considerably reduces the
 322 number of measurement points (between 229 and 1041, depending on the precision chosen
 323 to solve the integral). Moreover, the method directly uses the measured field and not its
 324 spatial Fourier transform. Compared to the previous unfiltered method using the Lebedev
 325 quadrature, the factor $1/j_n(k_0 r_S)$ (cf. Eq. (7)) generating an important error in the presence
 326 of noise does not appear in Eq. (38). Finally, this new filtered Lebedev method allows for the
 327 reconstruction of focused acoustic fields at the focal point by measuring them far from areas
 328 with strong amplitude dynamics, which is of interest for some dynamic-limited sensors.
 329 It is, however, restricted to progressive, harmonic fields propagating in free space, and
 330 requires the radius of the spherical surface to be large enough for the spherical Hankel
 331 functions and acoustic field approximations to hold.

332 B. Numerical validation

333 The filtered Lebedev method is applied to estimate the BSC of a focused vortex field
 334 described by Eq. (6), of frequency $f_0 = 50$ MHz, topological charge $m' = 1$, aperture angle
 335 $\alpha_0 = 50^\circ$ and focal distance $r_0 = 3$ mm propagating in water. The validation procedure
 336 consists in computing the acoustic field on the spherical surface of integration from the
 337 theoretical BSC truncated at $N = 50$. As before, random noise at 5% of the maximum
 338 amplitude of the field computed on the half-spherical surface is numerically added. Then,

Eq. (38) is solved using a Lebedev quadrature. Thus, the estimated BSC are compared to the theoretical ones, then used to compute the radiation force which is also compared to the theoretical one. This validation process allows determining the optimum numerical parameters, which are the integration sphere radius r_S and the Lebedev quadrature order. In a first step, the quadrature order is studied, the surface radius is set to 10λ , implying a truncation of $N = 30$. The reconstruction of the BSC as well as the calculation of the radiation force is performed for several orders of quadrature listed in the Table I, with the corresponding numbers of measurement points. The Lebedev quadrature is implemented numerically using the Python library *quadpy*.

348

Quadrature order	35	41	47	53	59	65	71	77
Number of points	229	309	401	505	621	749	889	1041

TABLE I. Orders of the Lebedev quadrature and associated numbers of points on the half-sphere defined by $\theta \geq \pi/2$.

350

The relative error on the estimation of the BSC is given by:

$$\epsilon(A_n^m) = \frac{100}{(N+1)(2N+1)} \sum_{n=0}^N \sum_{m=-n}^n \frac{|A_n^m - A_n^{m,th}|}{\max |A_n^{m,th}|} \quad (\%), \quad (39)$$

and by Eq. (25) for the force cylindrical component. The errors evolving with the order of the quadrature are plotted Fig. 6 (A). The BSC error is much weaker than those related to the radiation force and is stabilizing around 0.15% from a quadrature order of 59. On the other hand, the errors related to the cylindrical components of the force are not monotonic

355

and do not seem to have any specific relationship with the BSC error. The axial component is of particular importance here because, in the case of the vortex, it has the smallest amplitude compared to the others, about one order of magnitude less for the negative peak. However, the axial force is essential to obtain a three-dimensional trap, so interest will be focused on the error made on this component. In addition, we wish to minimise the number of points for the field in order to reduce the measurement duration. A compromise must therefore be made between the error and the number of points. The estimation error related to the axial force is minimal, about 1%, for an order of quadrature of 65 and 71, which corresponds to 749 and 889 points respectively (cf. Table I).

It is now appropriate to study the second parameter of interest, the radius r_S of the half-sphere of integration. This radius must be taken sufficiently large compared to the wavelength so that the asymptotic forms of the spherical Hankel functions hold. This condition numerically imposes $N < \pi r_S/\lambda$. Thus, the radius is varied between λ and 10λ , and N according to r_S (cf. Table II). Again, the error on the BSC, Fig. 6 (B), remains very small

r_S	1λ	2λ	3λ	4λ	5λ	6λ	7λ	8λ	9λ	10λ
N	3	6	9	12	15	18	21	25	28	30

TABLE II. Radii r_S of the half-sphere of integration and associated truncation orders N of the BSC series.

370
371

compared to those on the force and it stabilizes below 0.2% from a radius of 5λ . The errors on the force components seem to oscillate and reach local minimum values at odd radii. The

374 global minimum error on F_z corresponds to a radius of 7λ . The high errors occurring for
 375 radii below 5λ can be caused by an under sizing of the integration sphere and/or a too low
 376 truncation order.

377 The parameters finally retained (cf. Table III) are therefore a half-sphere of radius $r_S = 7\lambda$,
 378 allowing a truncation of the BSC series at $N = 21$, a minimum order of quadrature of 65
 379 and therefore 749 measurement points.

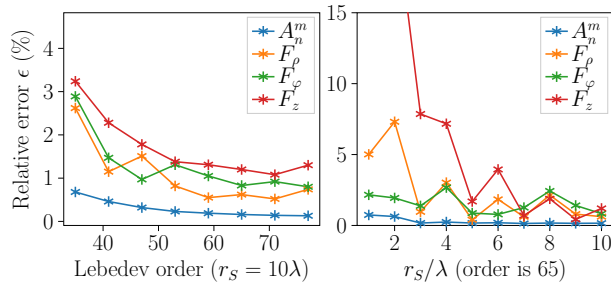


FIG. 6. (Color online) Relative errors of estimation of the filtered method based on the Lebedev quadrature, defined by Eq. (38). The errors for the BSC are computed from Eq. (39) and those for cylindrical components of the radiation force from Eq. (25). On the left the error is expressed in terms of the quadrature order of integration (cf. Table I) while the radius of the integration surface is set to 10λ (implying a truncation order of the BSC series of $N = 30$). On the right, the error is expressed in terms of the radius of the integration surface (cf. Table II) while the quadrature order is set to 65.

380
 382

383 C. Comparison with previous methods

384 The new filtered method can be compared to the unfiltered Lebedev method (cf. sec-
 385 tion II C 1) and to the filtered ASM (cf. section II C 2). The radius of the integration surface

Radius r_S	7λ
Truncation order N	21
Lebedev quadrature order	65
Number of points	749

TABLE III. Optimal parameters for the new Lebedev filtered method defined by Eq. (38).

386 is set to $5.6\lambda^{14}$ for the unfiltered Lebedev method. The truncation order N and the Lebedev
 387 quadrature order are identical to the new filtered method (cf. Table III). The filtered ASM is
 388 used on an acoustic field defined in the focal plane (located in $z = 0$) of dimensions $6\lambda \times 6\lambda$
 389 sampled in $61^2 = 3721$ measurement points, corresponding to a sampling step of $\lambda/10$.

390 The estimated forces by the three different methods are plotted in Fig. IV C. They all prop-
 391 erly recover the theoretical force, even though the error is slightly higher for the ASM. It
 392 can be reduced by increasing the size and number of points of the measurement plane. The
 393 axial force estimated by the unfiltered Lebedev method shows slight oscillations. These
 394 oscillations depend on the signal to noise ratio and the radius chosen for the quadrature.
 395 The noise acts partly as a standing wave, known to generate much stronger forces than a
 396 travelling wave²⁸. However, in the absence of filtering, the noise causes oscillations of the
 397 axial force, axis on which the focused vortex is progressive. On the contrary, radially $j_n(kr)$
 398 is the sum of two converging and diverging Hankel functions and can be considered as a
 399 standing field.

400 The new filtered Lebedev method therefore provides a low-cost, reliable, noise-insensitive

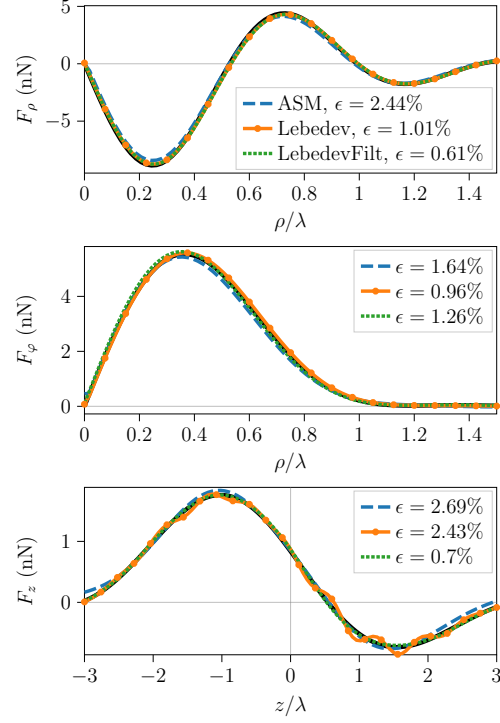


FIG. 7. (Color online) Comparison of the cylindrical components of the radiation force exerted on a $7 \mu\text{m}$ silica bead by a progressive focused vortex beam using the filtered ASM (with $z = 0$, and plane dimensions of $6\lambda \times 6\lambda$ sampled in 3721 points) (cf. Eq. (11)), the unfiltered Lebedev method (noted Lebedev, with parameters: $r_S = 5.6\lambda$ and a quadrature order of 65) (cf. Eq. (7)) and the filtered Lebedev method (noted LebedevFilt, with parameters listed in Table. III) (cf. Eq. (38)). The estimations are done with noise of amplitude up to 5% of the maximum pressure field computed on the surface of interest. Each estimated BSC series is truncated at $N = 21$. The theoretical force is plotted in black. The errors ϵ made by each method on the force are given by Eq. (25).

402 estimation of the BSC of the acoustic field that allows reconstruction of the radiation force
 403 with errors around 1% and lower than 1% for the axial component, while requiring a min-
 404 imal number of points compared to other methods. The advantages of this method are a
 405 spatial filtering of the standing waves which strongly reduces the influence of noise, a lim-

406 ited number of measurement points, chosen specifically for the numerical computation of
 407 the integral (cf. Eq. (38)), and the direct use of the measured field instead of its Fourier
 408 transform. Moreover, the absence of the $1/j_n$ term, which appears in the first unfiltered
 409 Lebedev method, also makes it much more stable.

410 Finally, the new method is applied to the acoustic tweezers described in previous works on

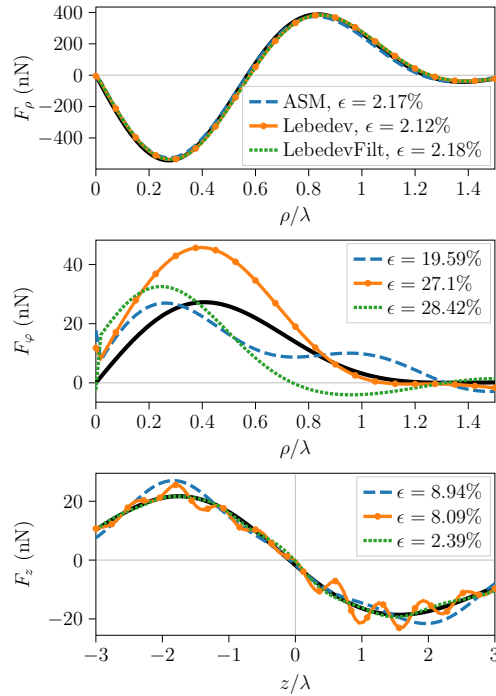


FIG. 8. (Color online) Comparison of the cylindrical components of the radiation force exerted on a 0.1λ polystyrene bead by a progressive focused vortex beam at frequency 1.2 MHz, aperture angle $\alpha_0 = 43^\circ$, focusing distance $r_0 = 75$ mm, topological charge $m' = 1$ and maximal amplitude 0.8 MPa¹⁴.

411

412

413 beam shape coefficients, see Ref.¹⁴. The vortex field parameters are $f_0 = 1.2$ MHz, $\alpha_0 = 43^\circ$,

414 $r_0 = 75$ mm, $m' = 1$ and its maximum amplitude is set to 0.8 MPa at the focal plane. As

415 before, the filtered ASM, the unfiltered and filtered Lebedev methods are used to recover

416 the BSC and compute the radiation force exerted on a polystyrene bead of radius 0.1λ (with
 417 $\lambda \approx 1.2$ mm in this case), density $\rho_p = 1080$ kg/m³, longitudinal velocity $c_L = 2350$ m/s
 418 and transverse velocity $c_T = 1120$ m/s. Same numerical parameters as before are used for
 419 the ASM and unfiltered Lebedev method, but for the filtered Lebedev method, the radius
 420 of the integration surface r_S is set to 10λ , resulting in a truncation order N of 25, while the
 421 quadrature order of integration is kept as before to 65. Noise is also added as before, to an
 422 amount of 5% of the maximum pressure amplitude.

423 Fig. 8 shows the radiation force recovered by the three previous methods and can be com-
 424 pared to Fig. 7 (left) of Ref.¹⁴. First, it is noticed that the radial component is equivalently
 425 recovered by all methods, with a 2% error. On the other hand, the azimuthal component
 426 is not recovered by any method. This component is progressive, defined by $e^{im'\varphi}$, and none
 427 of the methods described here are performing azimuthal filtering. Thus, they are all dis-
 428 turbed by noise for this component. Also, the high-frequency acoustic tweezers defined in
 429 the present work has an aperture angle of 50° , against 43° for the one defined in Ref.¹⁴. This
 430 results in stronger focusing for the 50 MHz tweezers and in better performance of the BSC
 431 determination methods, due to the reduced ratio between the progressive (along φ and z)
 432 and the standing (along ρ) waves. Note that the radial to azimuthal forces ratio is about
 433 20 in Ref.¹⁴ and is lower than 2 in the present work. Finally, we recall that the azimuthal
 434 force determination can be significantly improved by cancelling the BSC when $m \neq m'$, see
 435 the right of Fig. 7 in Ref.¹⁴.

436 Regarding the axial component of the force, it is best recovered by the new filtered Lebedev
 437 method, with an error lower than 3%. Both ASM and the unfiltered Lebedev method show

438 an error of around 9% on F_z . As noted before, the ASM does not display oscillations, con-
 439 trary to the Lebedev method. Moreover, these oscillations are enhanced by the diminution
 440 of the aperture angle inducing the increase of stationary effects. The radial to axial forces
 441 ratio is about 20 for $\alpha_0 = 43^\circ$ and about 5 for $\alpha_0 = 50^\circ$. In conclusion, the new filtered
 442 method is more efficient while requiring fewer measurement points. The filtering is all the
 443 more necessary as the beam is weakly focused.

444 V. CONCLUSION

445 Determination of the radiation force is an important process for the calibration of acoustic
 446 tweezers. A way to achieve this is to use a BSC determination method applied to a field mea-
 447 surement and then compute the associated force from the BSC A_n^m . Two kinds of methods
 448 have been previously described, unfiltered, e.g. the Lebedev method, and filtered methods,
 449 e.g. the ASM. The first method was proven to be very sensitive to noise, unlike the ASM, due
 450 to noise producing standing waves-like behavior. We showed that the good results obtained
 451 by the ASM are related to an implicit filtering of the standing waves. Indeed, this filtered
 452 method is failing to reconstruct the radiation force produced by a standing focused vortex
 453 beam. We presented a complete unfiltered ASM relevant for standing waves and capable of
 454 estimating the forces with an error smaller than 2% for the axial component, whereas the
 455 filtered ASM is failing. Nevertheless, spatial filtering is essential for the determination of the
 456 BSC of progressive fields. Although the filtered ASM is quite efficient, it is experimentally
 457 time-consuming owing to the large number of measurement points of the acoustic field. This
 458 may be critical. Indeed for high-frequency ultrasound focused field, the spatial features are

459 of the order of the wavelength, about ten micrometers. Scanning such field with a spatial
460 resolution of a few microns is possible with optical interferometers and a high numerical
461 aperture objective to focus the probe arm. However the contrast of the interferometer is
462 now very sensitive to any change of the focus. Therefore, the scan should be finished be-
463 fore the drift in time is significant. Thus, we introduced a new filtered BSC determination
464 method inspired by the Lebedev method. It allows a very accurate reconstruction of the
465 radiation force, with errors smaller than 1%, at a low cost in terms of number of measure-
466 ment points (half of what is required by the unfiltered Lebedev method). It is insensitive
467 to noise and does not require the use of Fourier transforms. This can avoid some errors
468 related to windowing and spatial sampling of the field. Scanning on a sphere centered at the
469 focus of a sharply focused beam reduces the required dynamic range of the measurement
470 sensor. Furthermore, it removes an additional step of numerical data manipulation. The
471 optimal parameters of this method are studied numerically. Experimental demonstration
472 for focused fields at 50 MHz, wavelength $30 \mu\text{m}$ and scanning with an optical interferometer
473 is underway. The experimental set-up and results will be reported in a subsequent paper.

474 **AUTHOR DECLARATIONS**

475 All authors declare they have no conflict of interest.

476 **DATA AVAILABILITY**

477 The data that support the findings of this study are available from the corresponding
478 author.

479 **REFERENCES**

480 ¹M. Baudoin and J.-L. Thomas, “Acoustic Tweezers for Particle and Fluid Microma-
481 nipulation,” *Annual Review of Fluid Mechanics* **52**(1), 205–234 (2020) doi: [10.1146/
482 annurev-fluid-010719-060154](https://doi.org/10.1146/annurev-fluid-010719-060154).

483 ²M. A. B. Andrade, N. Pérez, and J. C. Adamowski, “Review of Progress in Acous-
484 tic Levitation,” *Brazilian Journal of Physics* **48**(2), 190–213 (2018) doi: [10.1007/
485 s13538-017-0552-6](https://doi.org/10.1007/s13538-017-0552-6).

486 ³D. Baresch, J.-L. Thomas, and R. Marchiano, “Three-dimensional acoustic radiation force
487 on an arbitrarily located elastic sphere,” *The Journal of the Acoustical Society of America*
488 **133**(1), 25–36 (2013) doi: [10.1121/1.4770256](https://doi.org/10.1121/1.4770256).

489 ⁴D. Baresch, J.-L. Thomas, and R. Marchiano, “Spherical vortex beams of high radial
490 degree for enhanced single-beam tweezers,” *Journal of Applied Physics* **113**(18), 184901
491 (2013) doi: [10.1063/1.4803078](https://doi.org/10.1063/1.4803078).

492 ⁵D. Baresch, J.-L. Thomas, and R. Marchiano, “Observation of a Single-Beam Gradient
493 Force Acoustical Trap for Elastic Particles: Acoustical Tweezers,” *Physical Review Letters*
494 **116**(2), 024301 (2016) doi: [10.1103/PhysRevLett.116.024301](https://doi.org/10.1103/PhysRevLett.116.024301).

495 ⁶A. Marzo, M. Caleap, and B. W. Drinkwater, “Acoustic Virtual Vortices with Tunable
496 Orbital Angular Momentum for Trapping of Mie Particles,” *Physical Review Letters* **6**
497 (2018).

498 ⁷S. Vincent, P. Challande, and R. Marchiano, “Calibration of the axial stiffness of a single-
499 beam acoustic tweezers,” *Review of Scientific Instruments* **94**(9), 095102 (2023) doi: [10.](https://doi.org/10.1063/1.5044441)

500 [1063/5.0150610](#).

501 ⁸D. Baresch and V. Garbin, “Acoustic trapping of microbubbles in complex environments
502 and controlled payload release,” *Proceedings of the National Academy of Sciences* **117**(27),
503 15490–15496 (2020) doi: [10.1073/pnas.2003569117](#).

504 ⁹A. V. Nikolaeva, S. A. Tsysar, and O. A. Sapozhnikov, “Measuring the radiation force
505 of megahertz ultrasound acting on a solid spherical scatterer,” *Acoustical Physics* **62**(1),
506 38–45 (2016) doi: [10.1134/S1063771016010048](#).

507 ¹⁰M. A. Ghanem, A. D. Maxwell, O. A. Sapozhnikov, V. A. Khokhlova, and M. R. Bailey,
508 “Quantification of Acoustic Radiation Forces on Solid Objects in Fluid,” *Physical Review*
509 *Applied* **12**(4), 044076 (2019) doi: [10.1103/PhysRevApplied.12.044076](#).

510 ¹¹J. Lee, J. S. Jeong, and K. K. Shung, “Microfluidic acoustic trapping force and stiffness
511 measurement using viscous drag effect,” *Ultrasonics* **53**(1), 249–254 (2013) doi: [10.1016/](#)
512 [j.ultras.2012.06.008](#).

513 ¹²Y. Li, C. Lee, K. Ho Lam, and K. Kirk Shung, “A simple method for evaluating the
514 trapping performance of acoustic tweezers,” *Applied Physics Letters* **102**(8), 084102 (2013)
515 doi: [10.1063/1.4793654](#).

516 ¹³O. A. Sapozhnikov and M. R. Bailey, “Radiation force of an arbitrary acoustic beam on
517 an elastic sphere in a fluid,” *The Journal of the Acoustical Society of America* **133**(2),
518 661–676 (2013) doi: [10.1121/1.4773924](#).

519 ¹⁴D. Zhao, J.-L. Thomas, and R. Marchiano, “Computation of the radiation force exerted by
520 the acoustic tweezers using pressure field measurements,” *The Journal of the Acoustical*

521 Society of America **146**(3), 1650–1660 (2019) doi: [10.1121/1.5126095](https://doi.org/10.1121/1.5126095).

522 ¹⁵B. Rafaely, “The Spherical-Shell Microphone Array,” IEEE Transactions on Audio, Speech,
523 and Language Processing **16**(4), 740–747 (2008) doi: [10.1109/TASL.2008.920059](https://doi.org/10.1109/TASL.2008.920059).

524 ¹⁶A. Fahim, P. N. Samarasinghe, and T. D. Abhayapala, “Sound field separation in a mixed
525 acoustic environment using a sparse array of higher order spherical microphones,” in *2017*
526 *Hands-free Speech Communications and Microphone Arrays (HSCMA)*, IEEE, San Fran-
527 cisco, CA, USA (2017), pp. 151–155, doi: [10.1109/HSCMA.2017.7895580](https://doi.org/10.1109/HSCMA.2017.7895580).

528 ¹⁷D. L. Alon and B. Rafaely, “Spherical microphone array with optimal aliasing cancella-
529 tion,” in *2012 IEEE 27th Convention of Electrical and Electronics Engineers in Israel*,
530 IEEE, Eilat, Israel (2012), pp. 1–5, doi: [10.1109/EEEI.2012.6377007](https://doi.org/10.1109/EEEI.2012.6377007).

531 ¹⁸G. T. Silva, “An expression for the radiation force exerted by an acoustic beam with
532 arbitrary wavefront,” J. Acoust. Soc. Am. **130**(6), 3541–3544 (2011).

533 ¹⁹Z. Gong and M. Baudoin, “Equivalence between angular spectrum-based and multipole
534 expansion-based formulas of the acoustic radiation force and torque,” J. Acoust. Soc. Am.
535 **149**(5), 3469–3482 (2021) doi: [10.1121/10.0005004](https://doi.org/10.1121/10.0005004).

536 ²⁰A. Marzo, S. A. Seah, B. W. Drinkwater, D. R. Sahoo, B. Long, and S. Subramanian,
537 “Holographic acoustic elements for manipulation of levitated objects,” Nature Communi-
538 cations **6**(1), 8661 (2015) doi: [10.1038/ncomms9661](https://doi.org/10.1038/ncomms9661).

539 ²¹P. L. Marston, “Axial radiation force of a bessel beam on a sphere and direction reversal
540 of the force,” J. Acoust. Soc. Am. **120**(6), 3518 (2006).

541 ²²P. L. Marston, “Scattering of a bessel beam by a sphere: Ii. helicoidal case and spherical

- 542 shell example,” J. Acoust. Soc. Am. **124**(5), 2905–2910 (2008).
- 543 ²³L. Zhang and P. L. Marston, “Geometrical interpretation of negative radiation forces
544 of acoustical bessel beams on spheres,” Phys. Rev. E **84**(3, 2) (2011) doi: [10.1103/
545 PhysRevE.84.035601](https://doi.org/10.1103/PhysRevE.84.035601).
- 546 ²⁴L. Zhang, “A general theory of arbitrary bessel beam scattering and interactions with a
547 sphere,” J. Acoust. Soc. Am. **143**(5), 2796–2800 (2018) doi: [10.1121/1.5036734](https://doi.org/10.1121/1.5036734).
- 548 ²⁵M. A. Ghanem, A. D. Maxwell, Y.-N. Wang, B. W. Cunitz, V. A. Khokhlova, O. A.
549 Sapozhnikov, and M. R. Bailey, “Noninvasive acoustic manipulation of objects in a living
550 body,” Proceedings of the National Academy of Sciences **117**(29), 16848–16855 (2020) doi:
551 [10.1073/pnas.2001779117](https://doi.org/10.1073/pnas.2001779117).
- 552 ²⁶V. I. Lebedev and D. N. Laikov, “A quadrature formula for the sphere of the 131st algebraic
553 order of accuracy,” Doklady Mathematics **59**, 477–481 (1999).
- 554 ²⁷S. L. Sobolev, “Cubature Formulas on the Sphere Invariant under Finite Groups of Rota-
555 tions,” in *Selected Works of S.L. Sobolev*, edited by G. V. Demidenko and V. L. Vaskevich
556 (Springer US, Boston, MA, 2006), pp. 461–466, doi: [10.1007/978-0-387-34149-1_21](https://doi.org/10.1007/978-0-387-34149-1_21).
- 557 ²⁸L. V. King, “On the acoustic radiation pressure on spheres,” Proceedings of the Royal
558 Society of London. Series A - Mathematical and Physical Sciences **147**(861), 212–240
559 (1934) doi: [10.1098/rspa.1934.0215](https://doi.org/10.1098/rspa.1934.0215).
- 560 ²⁹P. M. Morse and H. Feshbach, *Methods of Theoretical Physics*, Vol. 1 (McGraw-Hill, 1953).
- 561 ³⁰I. S. Gradshteyn and I. M. Ryzhik, *Table of Integrals, Series and Products, Chap. 8 (Eq.*
562 *8.533.1)*, 7. ed. ed. (Elsevier Acad. Press, Amsterdam, 2009), p. 1171.

563 ³¹M. Abramowitz and I. Stegun, *Handbook of Mathematical Functions with Formulas,*
564 *Graphs, and Mathematical Tables*, Applied Mathematics Series (U.S. Government Printing
565 Office, 1948).

566 ³²J. Z. Buchwald and C.-P. YeangZhao, “Kirchhoff’s theory for optical diffraction, its prede-
567 cessor and subsequent development: the resilience of an inconsistent theory,” *Arch. Hist.*
568 *Exact Sci.* **70**(5), 463–511 (2016) doi: [10.1007/s00407-016-0176-1](https://doi.org/10.1007/s00407-016-0176-1).

569 ³³S. Schot, “80 years of sommerfeld’s radiation condition,” *Historia mathematica* **19**(4),
570 385–401 (1992) doi: [10.1016/0315-0860\(92\)90004-U](https://doi.org/10.1016/0315-0860(92)90004-U).